The Atmospheric Energy Constraint on Global-Mean Precipitation Change

ANGELINE G. PENDERGRASS AND DENNIS L. HARTMANN

Department of Atmospheric Sciences, University of Washington, Seattle, Washington

(Manuscript received 7 March 2013, in final form 6 September 2013)

ABSTRACT

Models from phase 5 of the Coupled Model Intercomparison Project (CMIP5) robustly predict that the rate of increase in global-mean precipitation with global-mean surface temperature increase is much less than the rate of increase of water vapor. The goal of this paper is to explain in detail the mechanisms by which precipitation increase is constrained by radiative cooling. Changes in clear-sky atmospheric radiative cooling resulting from changes in temperature and humidity in global warming simulations are in good agreement with the multimodel, global-mean precipitation increase projected by GCMs ($\sim$1.1 W m^{-2} K^{-1}).

In an atmosphere with fixed specific humidity, radiative cooling from the top of the atmosphere (TOA) increases in response to a uniform temperature increase of the surface and atmosphere, while atmospheric cooling by exchange with the surface decreases because the upward emission of longwave radiation from the surface increases more than the downward longwave radiation from the atmosphere. When a fixed relative humidity (RH) assumption is made, however, uniform warming causes a much smaller increase of cooling at the TOA, and the surface contribution reverses to an increase in net cooling rate due to increased downward emission from water vapor. Sensitivity of precipitation changes to lapse rate changes is modest when RH is fixed. Carbon dioxide reduces TOA emission with only weak effects on surface fluxes, and thus suppresses precipitation. The net atmospheric cooling response and thereby the precipitation response to CO_2-induced warming at fixed RH are mostly contributed by changes in surface fluxes. The role of clouds is discussed.

Intermodel spread in the rate of precipitation increase across the CMIP5 simulations is attributed to differences in the atmospheric cooling.

1. Introduction

Precipitation is an important driver of the dynamics of climate and the biosphere, and is of great practical importance to society. Climate models robustly predict an increase in global-mean precipitation in response to CO_2 doubling. They agree that the magnitude of this increase will be less than the increase of water vapor concentrations (Held and Soden 2006). This is true for the multimodel mean, as well as for individual models (although the variation across models is large). The projected rate of increase of global-mean precipitation has long been attributed to the atmospheric energy budget constraint, but the mechanisms and sensitivities of this constraint have yet to be thoroughly explained. Here we calculate changes in clear-sky atmospheric radiative cooling and relate them to the projected global-mean precipitation change. The relative importance of surface and top of the atmosphere (TOA) fluxes is illustrated, and the critical importance of downward emission by water vapor is shown. Although the global-mean precipitation change is less important to humans than regional changes, the global constraint affects the regional responses.

On time scales longer than a year, atmospheric energy constrains precipitation. Latent heating of the atmosphere must be balanced by atmospheric cooling, which is primarily radiative. This idea was popularized by Allen and Ingram (2002). They separated radiative cooling change into two components: one due to a forcing (e.g., CO_2) and another that depends on the change in surface temperature. They used calculations from the GCM experiments in Mitchell et al. (1987) to quantify the magnitude of these two terms, and showed that the atmospheric cooling predicted by this calculation fit the precipitation increase in model experiments from the Coupled Model Intercomparison Project (CMIP) phase 2 (CMIP2).

Since Allen and Ingram (2002), a number of studies have addressed the energetic constraint on precipitation.

Corresponding author address: Angeline G. Pendergrass, University of Washington, Box 351640, Seattle, WA 98195.
E-mail: angie@atmos.washington.edu

DOI: 10.1175/JCLI-D-13-00163.1

Takahashi (2009b) developed a radiative–convective equilibrium model that highlighted the interplay between radiative and sensible heat flux, as well as changes in near-surface stability and relative humidity, in determining precipitation change. Lambert and Webb (2008) showed that in an ensemble of GCMs with perturbed physics, the precipitation change due to CO_2 doubling was strongly related to clear-sky atmospheric radiation. Allan (2006) examined observations of clear-sky radiative cooling. Stephens and Ellis (2008) examined changes in precipitation due to transient CO_2 increase in Intergovernmental Panel on Climate Change (IPCC) Fourth Assessment Report (AR4) models. They calculated atmospheric radiation from an empirical relationship with column water vapor, preventing the separation of responses to warming and moistening. Previdi (2010) calculated the atmospheric radiative responses to AR4 GCM warming and moistening using feedback kernels. We aim to build upon these studies by providing a simple and understandable account of clear-sky atmospheric cooling response to warming and moistening.

This paper will proceed as follows. First, we present the change in global-mean precipitation in transient CO_2 increase experiments from phase 5 of CMIP (CMIP5). Next, we construct a framework for the global-mean atmospheric radiative energy balance. This framework consists of the atmospheric cooling response to idealized changes in temperature, moisture, and CO_2 forcing. The atmospheric radiative cooling calculations allow us to attribute the changes in clear-sky radiative fluxes seen in GCMs to the structure of changes in temperature, water vapor, and CO_2. We compare the sum of these changes to the clear-sky fluxes in the CMIP5 multimodel mean to ensure fidelity of our framework, and reconcile the framework with CMIP5 precipitation changes. Then we examine the intermodel spread in the rate of precipitation increase across models. In the last section, we discuss the role of clouds, aerosol forcing, and the surface perspective on precipitation change.

2. Atmospheric energy and precipitation change

The atmosphere exchanges energy via turbulent fluxes of heat and moisture with the surface, and radiatively with both the surface and space. The global-mean atmospheric energy budget, E_a, is described by Eq. (1):

$$\frac{dE_a}{dt} = \mathrm{LE} + \mathrm{SH} + R. \tag{1}$$

Latent heat flux (LE) enters the atmosphere through evaporation of water from the surface. The water budget is in balance on interannual and longer time scales, so evaporation and precipitation must be equal. Therefore the latent heat flux entering the atmosphere must be equal to LP, when the latent heat of condensation of water L is multiplied by the rain rate P ($\mathrm{kg\,m^{-2}\,s^{-1}}$). Sensible heat flux (SH) is the turbulent transfer of heat from the surface to the atmosphere. The atmospheric column net radiation, R, is the sum of net radiant energy entering the atmosphere through its top (the TOA) and its bottom (the earth's surface). We can quantify these terms by examining the multimodel mean from 10 years of CMIP5 simulations. In these simulations, on average, LP is $85\,\mathrm{W\,m^{-2}}$, SH is $20\,\mathrm{W\,m^{-2}}$, and R is $-105\,\mathrm{W\,m^{-2}}$, and these terms balance since storage of energy in the atmosphere is small.

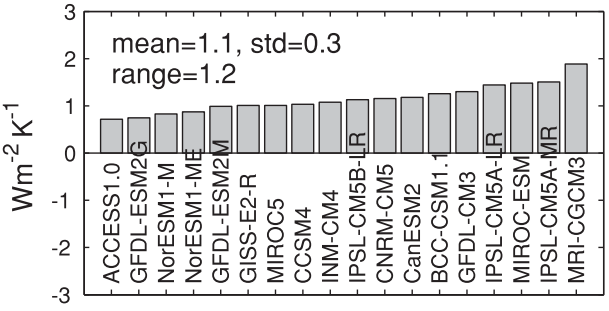

FIG. 1. Global-mean precipitation sensitivity in CMIP5 models ($\mathrm{W\,m^{-2}\,K^{-1}}$), estimated from the difference between first 10 years and years 61–70 in the transient CO_2 increase scenario.

Latent and sensible heat fluxes transfer energy to the atmosphere from the surface, and the atmospheric radiation removes this energy. If any one of these three terms changes, the other terms change to maintain balance. In the bulk of this paper we will focus on how R and LP balance.

First, we examine how LP changes in response to CO_2 forcing in GCMs. Global-mean precipitation increase in transient CO_2 increase experiments (1pctCO2; Taylor et al. 2012) is shown in Fig. 1 for each of the CMIP5 models used throughout this paper. Only models with available precipitation, total-sky and clear-sky radiation at the surface and TOA, and atmospheric and near-surface air temperature and moisture fields are used, and only one ensemble member from each model is included. Time differences are taken between years 1–10 and years 61–70 of the experiments (year 70 is the time of CO_2 doubling; some models stop after this). For each model, the precipitation change is normalized by the change in global-mean surface air temperature.

All models show an increase in precipitation, although the variation in magnitude across models is large. The multimodel mean precipitation increase is $1.1\,\mathrm{W\,m^{-2}\,K^{-1}}$, which corresponds to 1.4% of the multimodel, global-mean precipitation. This is much less than the rate of

TABLE 1. CMIP5 multimodel, global-mean change (Δ) in energy components for transient CO_2 increase ($W\,m^{-2}\,K^{-1}$) calculated directly from GCMs. Positive signs correspond to increasing precipitation. Here T is the surface air temperature, LP is precipitation times the latent heat of vaporization of water, SH is sensible heat flux, R_{atm} is atmospheric radiative cooling, cs indicates clear sky, cloud indicates cloudy sky, and R_{TOA} is the TOA outgoing radiative response.

$L\Delta P/\Delta T$	1.1
$\Delta SH/\Delta T$	0.3
$\Delta R_{atm,cs}/\Delta T$	1.2
$\Delta R_{atm,cloud}/\Delta T$	−0.4
$\Delta R_{atm}/\Delta T$	0.8
$\Delta R_{TOA}/\Delta T$	−0.7

increase of water vapor, about $7\%\,K^{-1}$, which would correspond to $6\,W\,m^{-2}\,K^{-1}$ of precipitation increase. The change in multimodel, global-mean precipitation and other energy fluxes of interest are listed in Table 1. In the next section, we examine changes in atmospheric cooling, which we will later reconcile with the multimodel mean precipitation increase.

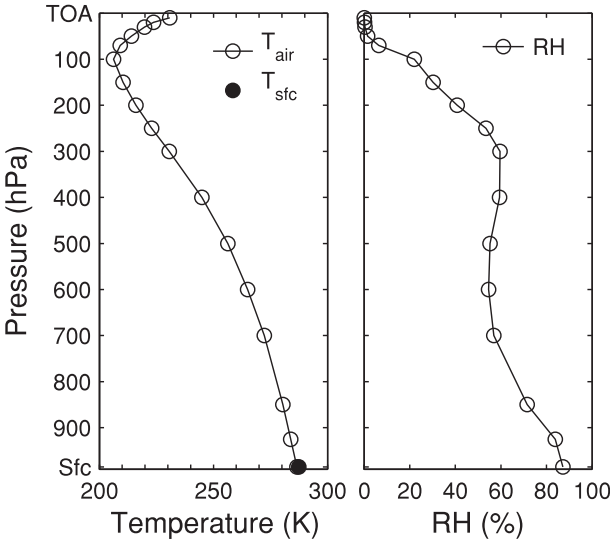

FIG. 2. Global mean of the CMIP5 multimodel mean temperature and RH profiles used as the baseline for column radiation calculations.

3. Atmospheric column radiative responses to idealized changes in temperature, moisture, and CO_2

a. Clear-sky radiative column calculations

Since the energy constraint on precipitation is fundamentally radiative, it can be explored in a simple radiative context. In this section, we calculate the atmospheric column radiative response to idealized changes in temperature, moisture, and CO_2 increase. For baseline calculations, we use annual mean profiles of temperature and specific humidity at each point on the globe from the CMIP5 multimodel mean for the first 10 years of the transient CO_2 increase experiment (global mean shown in Fig. 2). The multimodel mean is interpolated onto a common grid with 90 latitude and 144 longitude points. Archived CMIP5 model fields share a common pressure grid with 17 vertical pressure levels, although at many locations some of these levels are below the surface. At each location, our calculations include all standard levels that are above the multimodel, annual mean surface pressure. We also specify the bottom atmospheric level to be at the surface pressure and surface air temperature, with surface air specific humidity. We use CMIP5 multimodel mean ozone profiles (although only six of the models have archived ozone). For the surface layer, we set ozone the same as the level above it. We calculate radiative fluxes with the Fu and Liou (1992) column radiation model. To have meaningful shortwave (SW) components, we use the zonal, annual mean insolation-weighted solar zenith angle. Clouds are not included.

From this baseline radiative calculation, we incrementally vary temperature, moisture, and CO_2. We will consider them in turn, but the resulting atmospheric radiative responses are shown in Table 2. The sign is chosen so that an increase in atmospheric radiation corresponds to an increase in precipitation; that is, a positive change means more cooling. Since the atmospheric column response is the sum of the familiar TOA response and the surface response, the table also includes the TOA and surface responses.

We begin with an increase of atmospheric temperature by 1 K at all levels in the troposphere. The tropopause is defined as 100 hPa at the equator and 300 hPa at the poles, and is linearly interpolated in between. In the first line of Table 2, we see that atmospheric warming results in an increase in atmospheric longwave (LW) cooling of $5.6\,W\,m^{-2}\,K^{-1}$. Somewhat less than half of this cooling leaves from the TOA, and somewhat more than half is emitted toward the surface. This is an expected consequence of increasing the temperature of the atmosphere. The noteworthy aspect of this calculation is that the downward emission from the atmosphere to the surface is large, even larger than the change at the TOA.

In the second calculation (line 2 of Table 2), the atmosphere is returned to its baseline profile and the surface temperature is increased by 1 K. This results in an increase in LW emission from the surface of $5.0\,W\,m^{-2}\,K^{-1}$. Twenty-four percent of this radiation ($1.2\,W\,m^{-2}\,K^{-1}$) escapes to space through the TOA, and

TABLE 2. Clear-sky radiative response to various temperature, moisture, and CO_2 changes at the TOA, surface (SFC), and in the atmospheric column (ATM; $W m^{-2} K^{-1}$) calculated with Fu and Liou (1992) column radiation code. Signs are chosen so that a positive response contributes to increasing precipitation: increased cooling is positive for the atmospheric column, upwelling is positive at the TOA, and downwelling is positive at the surface. Note that the atmospheric cooling is the sum of net downwelling surface radiative flux and net upwelling TOA radiative flux: ATM = SFC + TOA. The two values of net change in clear-sky atmospheric radiative cooling are in boldface.

		TOA	SFC	ATM
1	Vertically uniform T_a	2.3	3.3	5.6
2	T_s	1.2	−5.0	−3.8
3	Vertically uniform warming	3.4	−1.7	1.8
4	LW fixed RH q	−1.7	3.4	1.7
5	Vertically uniform T, fixed RH, LW	1.8	1.7	3.4
6	SW fixed RH q, fixed RH	−0.1	−0.9	−1.0
7	Vertically uniform Net	1.7	0.8	2.5
8	Vertically varying T, idealized	0.7	−0.1	0.6
9	Vertically varying T, fixed RH q	0.0	−0.1	−0.1
10	Cumulative net	1.7	0.7	2.4
11	Transient CO_2	−2.0	0.9	−1.1
12	Net idealized response	−0.3	1.5	**1.2**
13	Vertically varying T, CMIP5	0.7	0.1	0.9
14	Vertically varying T, fixed RH q	0.1	0.3	0.3
15	Cumulative net	1.8	1.0	2.8
16	Transient CO_2	−2.0	0.6	−1.4
17	Net CMIP5 response	−0.3	1.6	**1.3**
18	ΔRH	0.1	−0.1	−0.0

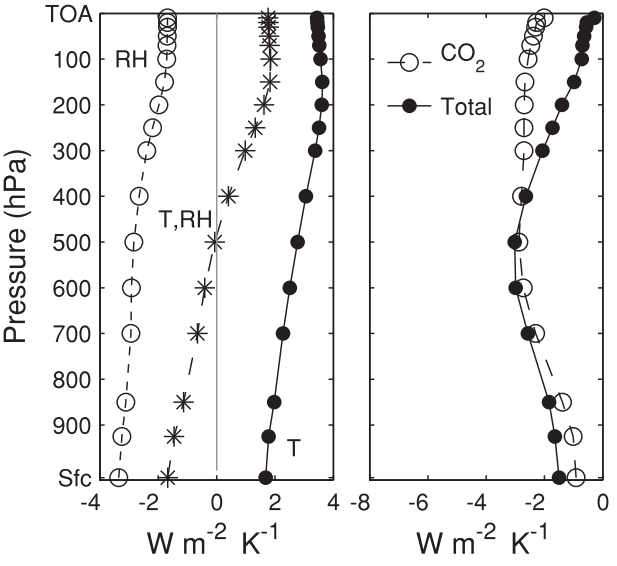

FIG. 3. Net upwelling radiative response ($W m^{-2} K^{-1}$). (left) LW responses to air and surface temperature increase of 1 K (filled circles), constant RH moisture increase (open circles), and combined temperature and moisture increase (asterisks). (right) Net upwelling radiative responses to CO_2 forcing (open circles) and warming, moistening, and CO_2 forcing combined (solid circles).

the rest is absorbed by the atmosphere. This is in agreement with a recent calculation of the fraction of surface emission emitted to space by Costa and Shine (2012), who calculated clear-sky transmission of 25%, although this is reduced to about 10% when clouds are included.

Typical warming includes changes in both the surface and the atmosphere. The third calculation is uniform warming of the surface and each atmospheric level by 1 K, which we refer to as ''uniform'' warming. Responses are listed in the third line of Table 2; Fig. 3 (left panel, solid line with filled circles) shows the change in net upwelling radiation at the surface, each level in the atmosphere, and the TOA due to the warming. The change in surface emission is higher than the change in downward atmospheric emission because the surface temperature is higher than the temperature at the effective atmospheric downward emission level. The overall effect of uniform warming is LW cooling of the atmosphere by $1.8 W m^{-2} K^{-1}$. Nearly double this amount of LW is lost from the TOA, but increased heating of the atmosphere by surface LW emission mitigates the TOA loss. Note the linearity of the temperature changes: the response to uniform warming differs from the sum of responses to warming the surface and atmosphere separately by just $0.1 W m^{-2} K^{-1}$.

Next we vary the moisture. First, the moisture is increased by the amount that would maintain constant relative humidity (RH) during a 1-K uniform warming, but the atmosphere and surface temperatures are maintained at their baseline values. The LW responses are tabulated in the fourth line of Table 2 and shown in Fig. 3 (left panel, short-dashed line with open circles). At the surface, downward emission from the atmosphere increases by $3.4 W m^{-2} K^{-1}$ as the increased water vapor lowers the effective height of emission to a warmer level. At the TOA, $1.7 W m^{-2} K^{-1}$ less LW is lost to space as the level of emission is raised to a cooler level. The overall LW atmospheric response to this moistening is $1.7 W m^{-2} K^{-1}$, an increase very similar in magnitude to the uniform warming increase. So the increase in humidity increases the radiative cooling of the atmosphere through increased downward emission to the surface. We infer from this that the precipitation rate in equilibrium is sensitive to the vertical distribution of humidity. Increased humidity in the lower troposphere contributes to increases in precipitation, while increased humidity in the upper troposphere contributes to decreases in precipitation. The wavelengths of water vapor continuum absorption are most important in determining surface emission, while upper tropospheric emission is determined by the wavelengths of rotation and vibrational bands (Mitchell et al. 1987; Inamdar et al. 2004).

The fifth line of Table 2 lists the LW response to uniform increase in temperature along with moistening at constant RH; this is also shown in Fig. 3 (left panel, long-dashed line with asterisks). Atmospheric cooling is increased by $3.4\,\mathrm{W\,m^{-2}\,K^{-1}}$, with the largest contributions coming from an increase in outgoing LW radiation (OLR) at the TOA due to warming and an increase in LW emission to the surface due to moistening. In contrast, uniform warming decreases emission to the surface and moistening decreases cooling to space.

We next take SW changes into account, which come into play because water vapor absorbs SW radiation. Line 6 of Table 2 shows the change in SW absorption due to constant-RH moistening for 1-K warming. SW absorption offsets the increased LW cooling by $1.0\,\mathrm{W\,m^{-2}\,K^{-1}}$. Line 7 of Table 2 lists the net response to the uniform warming with constant RH moistening. The net effect of uniform warming and constant RH moistening is an increase in atmospheric radiative cooling of $2.5\,\mathrm{W\,m^{-2}\,K^{-1}}$.

Models and theory predict that warming is amplified with height, rather than vertically uniform. To incorporate the variation of warming with height, we calculate the difference between moist adiabats starting from the initial and warmed surface air temperature. The OLR response to the variation in warming with height is the lapse rate feedback.

Lines 8–10 of Table 2 show the response to vertical variations in warming with height (minus the response to uniform warming); this is also shown in Fig. 4. Amplified warming with height enhances atmospheric cooling by $0.6\,\mathrm{W\,m^{-2}\,K^{-1}}$, mostly by increasing cooling to space from the warmer upper troposphere, but there is also $0.1\,\mathrm{W\,m^{-2}\,K^{-1}}$ of decreased cooling to the surface. Constant-RH moistening mitigates the OLR increase to just $-0.1\,\mathrm{W\,m^{-2}\,K^{-1}}$. Using the CMIP5 multimodel mean change in warming with height instead of the moist adiabatic approximation (lines 13–15 of Table 2) gives a change that is slightly larger, with $0.3\,\mathrm{W\,m^{-2}\,K^{-1}}$ more increase in atmospheric cooling.

So far we have considered uniform and vertically amplified warming, and moistening at constant RH. Now we must account for the radiative effect of the CO_2 forcing. We choose an initial CO_2 concentration corresponding to the mean of the first 10 years, 297.9 ppm, and a final concentration corresponding to the mean of years 61–70, 541.2 ppm. We incorporate stratospheric cooling due to the CO_2 forcing by using CMIP5 multimodel mean stratospheric temperatures. The mean temperature from years 61–70 is applied at all levels above the tropopause, which we define as a linear interpolation between 100 hPa at the equator and 300 hPa at the poles (following Soden and Held 2006; Previdi

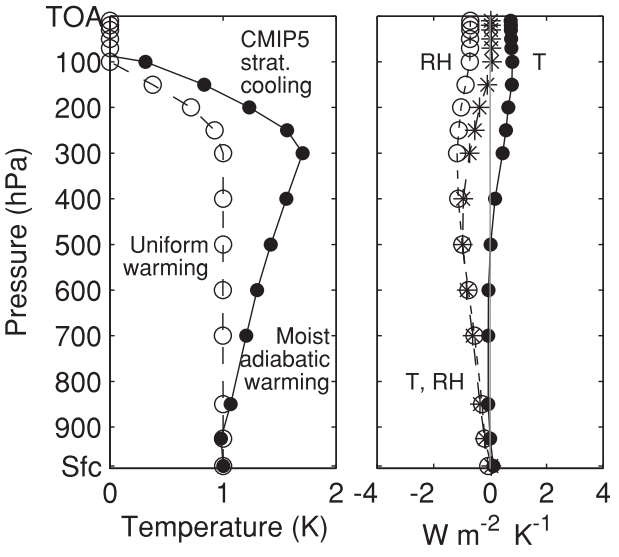

FIG. 4. (left) Amplification of warming with height, with global-mean vertical temperature increase for uniform warming (open circles) and warming amplified with height (the difference between moist adiabats, filled circles). (right) LW upwelling radiative response ($\mathrm{W\,m^{-2}\,K^{-1}}$) to amplified warming with height, with temperature increase alone (filled circles), constant-RH moistening alone (open circles), and warming and moistening together (asterisks).

2010). The response to CO_2 forcing is listed on line 11 of Table 2 and shown in Fig. 3 (right panel, dashed line with open circles). The CO_2 increase reduces cooling from the TOA by $2.0\,\mathrm{W\,m^{-2}\,K^{-1}}$, and also increases cooling to the surface by $0.9\,\mathrm{W\,m^{-2}\,K^{-1}}$. The overall effect is a reduction of atmospheric cooling by $1.1\,\mathrm{W\,m^{-2}\,K^{-1}}$.

Combining the CO_2 forcing and responses to uniform and amplified warming and constant-RH moistening, we obtain $1.2\,\mathrm{W\,m^{-2}\,K^{-1}}$ of increased atmospheric cooling calculated from our radiative transfer model. This is the same as the clear-sky atmospheric cooling change in the CMIP5 multimodel mean. We will return to this result and compare it with CMIP5 precipitation change in section 5.

The calculations in this section connect a set of simple, easily understandable changes in temperature and moisture to changes in atmospheric radiative cooling. Using these annual-mean, clear-sky profiles, we get reasonably close to CMIP5 precipitation change. Furthermore, they show how TOA radiative responses relate to the radiative response in the atmospheric column.

In the remaining lines of Table 2, we repeat lines 8–12 using the CMIP5 multimodel mean change in temperature with height, instead of the moist adiabatic warming. The net atmospheric cooling response differs by $0.1\,\mathrm{W\,m^{-2}\,K^{-1}}$, while individual components vary by up to $0.3\,\mathrm{W\,m^{-2}\,K^{-1}}$.

Additionally, we calculated the radiative effect of the CMIP5 multimodel mean change in RH, shown in line 18 of Table 2. The change in RH is determined from the model changes in specific humidity, in contrast to the assumption of constant RH that we use in the rest of the calculations. RH in the lowest layer of the atmosphere increases slightly over ocean, by less than $2\%\,K^{-1}$, whereas it decreases over land, typically by about $2\%\,K^{-1}$. The change in RH results in a decrease of $0.1\,W\,m^{-2}\,K^{-1}$ of net downwelling radiation to the surface because the decreasing near-surface RH over land dominates the increasing RH over ocean in the global mean. The decrease in emission to the surface is compensated by an increase in OLR of $0.1\,W\,m^{-2}\,K^{-1}$, so there is no net change in atmospheric cooling.

Previdi (2010) made similar calculations using the radiative feedback kernel technique. He found that the LW atmospheric cooling response to increased water vapor is a decrease in atmospheric cooling, dominated by the upper and middle tropospheric moistening. We find just the opposite, an increase in atmospheric LW cooling due to increased water vapor. Using the same clear-sky water vapor feedback kernels as that study with the multimodel mean moistening here, the change in atmospheric LW cooling is $-0.7\,W\,m^{-2}\,K^{-1}$, as compared to $1.1\,W\,m^{-2}\,K^{-1}$ calculated with Fu and Liou (1992) code. This direct comparison is with the same temperature and humidity profile, so the difference is due to the methodology or radiative transfer code. We think our calculation is accurate because we recover the change in clear-sky atmospheric radiative cooling from GCMs. Additionally, our finding that moistening increases atmospheric LW cooling is in agreement with variability seen in satellite and reanalysis data (Allan 2006).

b. Consistency of radiative column calculations and GCM fluxes

The calculations above show that the dominant mode of temperature and moisture change for setting the atmospheric radiative cooling response is the vertically uniform warming with fixed RH moistening. Now we are in a position to reconcile the magnitude of atmospheric radiative cooling response in our framework with global-mean precipitation change projected by CMIP5 models. Returning to line 12 of Table 2, we would expect to see $1.2\,W\,m^{-2}\,K^{-1}$ of precipitation change for the transient CO_2 response. We can compare this to the tabulated multimodel, global-mean changes in precipitation as well as atmospheric cooling listed in Table 1. Our calculation agrees with the CMIP5 multimodel mean clear-sky atmospheric radiative cooling change of $1.2\,W\,m^{-2}\,K^{-1}$. The alternative calculation using CMIP5 patterns of change agrees to within $0.1\,W\,m^{-2}\,K^{-1}$.

TABLE 3. Comparison of clear-sky radiative fluxes calculated with Fu and Liou (1992) column radiation code and CMIP5 multimodel mean radiative fluxes ($W\,m^{-2}\,K^{-1}$).

	Fu–Liou (moist adiabat)	Fu–Liou (CMIP5 fields)	CMIP5
ATM Net	1.2	1.3	1.2
LW	2.3	2.4	2.4
SW	−1.1	−1.1	−1.2
TOA LW	−0.2	−0.2	−0.3
Surface LW	2.5	2.6	2.6

We can also compare the clear-sky LW and SW radiative flux changes from the CMIP5 multimodel mean with our calculations. Table 3 shows this comparison. For atmospheric column cooling, the radiative column calculations agree with the CMIP5 multimodel mean to within $0.1\,W\,m^{-2}\,K^{-1}$. For the TOA and surface, only LW comparison is shown. We expect the SW to differ because we have not incorporated changes in the surface albedo, especially sea ice, but this should not affect the atmospheric column much. At the TOA and surface, our values agree to within $0.1\,W\,m^{-2}\,K^{-1}$.

While the effect of clouds on atmospheric radiation cannot be obtained in our annual-mean framework, we can consider how clouds influence the atmospheric cooling rate calculated by the GCMs. We will do this in section 5a.

c. Radiative column calculations of idealized clouds

Clouds play an undeniable role in the atmospheric energy budget. Figure 5 shows a column radiation calculation with two idealized clouds: a low cloud and a high cloud. We use global-mean profiles of temperature, moisture, and ozone for this calculation. Each cloud has a liquid water path of $40\,g\,m^{-2}$ and effective droplet radii of $14\,\mu m$. The low cloud occupies one pressure layer, from about 1.5 to 3 km. The high cloud occupies multiple layers, from 5.5 to 12 km. The liquid water is spread evenly across the layers. Ice is not considered. The clouds have SW optical depth of 0.5. The radiative responses to these clouds are listed in Table 4.

Here we encounter one of the great advantages of the atmospheric energy budget perspective over the surface perspective: reflection of SW by clouds has little effect on the atmospheric energy budget. There is a modest change in SW absorption when clouds are present, but this is far overwhelmed by the clouds' effects in the LW.

Consider the low cloud (left panel, Fig. 5). The low cloud has a LW emissivity near 1, causing the LW emission to the surface to come from a warmer temperature than it would in clear skies. This enhances atmospheric cooling to the surface. The cloud also intercepts LW emitted from the surface that would otherwise escape to space, decreasing the OLR and mitigating the increase in

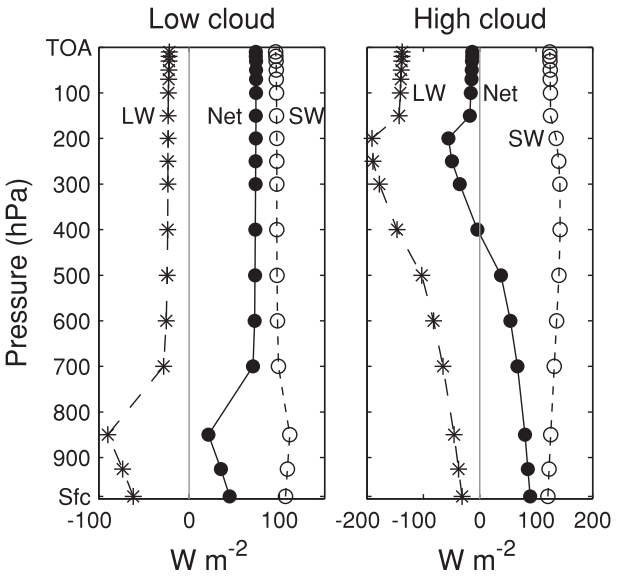

FIG. 5. Upwelling radiative response ($W m^{-2}$) to idealized clouds, for (left) low cloud and (right) high cloud. LW is shown with asterisks, SW with open circles, and net radiation with filled circles. Both clouds have liquid water path of $40 g m^{-2}$ and effective radius $14 \mu m$.

atmospheric cooling. The temperature difference between the surface and cloud top is relatively small, so that the increased emission to the surface dominates over the reduced OLR. Overall, the low cloud increases atmospheric cooling by $29 W m^{-2}$.

The high cloud changes surface LW by only a small amount, by emitting some LW downward from its base (Fig. 5, right panel). It has a much larger effect on the OLR. The cloud traps the LW emitted by the surface and warmer parts of the atmosphere, re-emitting radiation from its cold top. The overall effect is strong atmospheric heating, with a magnitude of $103 W m^{-2}$. The high cloud suppresses precipitation very strongly.

Clouds also affect radiation at the surface. In Fig. 5, the effect of the cloud on surface energy is the absolute difference at the bottom of the panel (the effect on the atmosphere is the slope of the line between the surface and TOA). Unlike for the atmospheric column, both low and high clouds have a large effect on the surface SW, of about $100 W m^{-2}$. For the low cloud, the reduction in SW is mitigated by an increase in absorbed LW. There is less mitigation for the high cloud.

4. Intermodel spread in atmospheric radiative cooling response to CO_2 forcing

In the previous section, we carefully examined the CMIP5 multimodel mean atmospheric cooling response to increasing CO_2 in order to understand the change in multimodel mean precipitation. Can we also understand the differences in the rate of precipitation increase across models? The range of climate response across models is often used to explore mechanisms for climate change. Previous studies have explored the intermodel spread in precipitation change due to climate forcing. Takahashi (2009a) examined the precipitation response in slab-ocean experiments from phase 3 of CMIP (CMIP3) forced by a doubling of CO_2. Previdi (2010), Pendergrass and Hartmann (2012), and others examined precipitation change in the realistic A1b forcing scenario in CMIP3, which included changes in aerosol forcing, and found that the difference in aerosol forcing dominates the intermodel spread. Here we consider the intermodel spread in precipitation response to the CO_2 forcing alone.

TABLE 4. Radiative response ($W m^{-2}$) to idealized clouds. As in previous tables, signs are chosen so that increased atmospheric cooling is positive.

	TOA	SFC	ATM
Low cloud LW	−22	62	40
SW	96	−107	−11
Net	74	−45	29
High cloud LW	−137	31	−106
SW	124	−121	3
Net	−13	−89	−103

Precipitation increase varies across the 18 models by a factor of 2 (Fig. 1). Change in precipitation is balanced by the sum of changes in sensible heat flux, cloud radiative forcing, and clear-sky atmospheric radiative cooling. Cloud radiative forcing change has a range of $1.2 W m^{-2} K^{-1}$ across models. Precipitation change is closely tied to the change in clear-sky radiative cooling alone in most models (Fig. 6). Omitting two outlier models, the correlation between precipitation change and clear-sky atmospheric radiative cooling is 0.91. The strong relationship of $\Delta R_{cs}/\Delta T$ with $\Delta P/\Delta T$ indicates that much of the intermodel spread in precipitation can be understood from changes in clear-sky atmospheric radiative cooling.

We calculate the clear-sky radiative cooling response to each model's pattern of warming and moistening, using the same procedure as in section 3. When compared to fluxes directly output from the GCMs, our calculations do a tolerable job at recovering the response of clear-sky LW atmospheric cooling (per degree global-mean surface temperature increase) calculated by the models ($r = 0.77$, slope = 0.6), but they do a poor job capturing the change in clear-sky SW absorption (Fig. 7). The calculated change in the multimodel mean matches quite closely, but there is very little spread in the SW absorption in our calculation, despite a range of

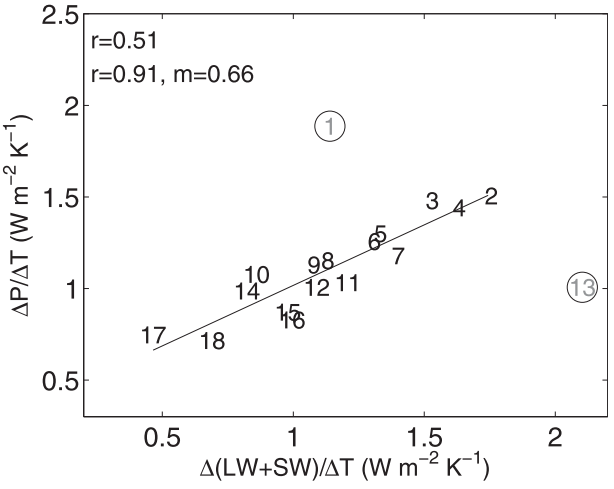

FIG. 6. Change in clear-sky atmospheric radiative cooling (from model output radiative fluxes) vs change in global-mean precipitation increase, normalized by global-mean surface temperature change for each CMIP5 model. Correlation is calculated with and without two outlier models, Goddard Institute for Space Studies Model E2-R (GISS E2-R) and Meteorological Research Institute Coupled General Circulation Model, version 3 (MRI CGCM3); slope is calculated without the outliers.

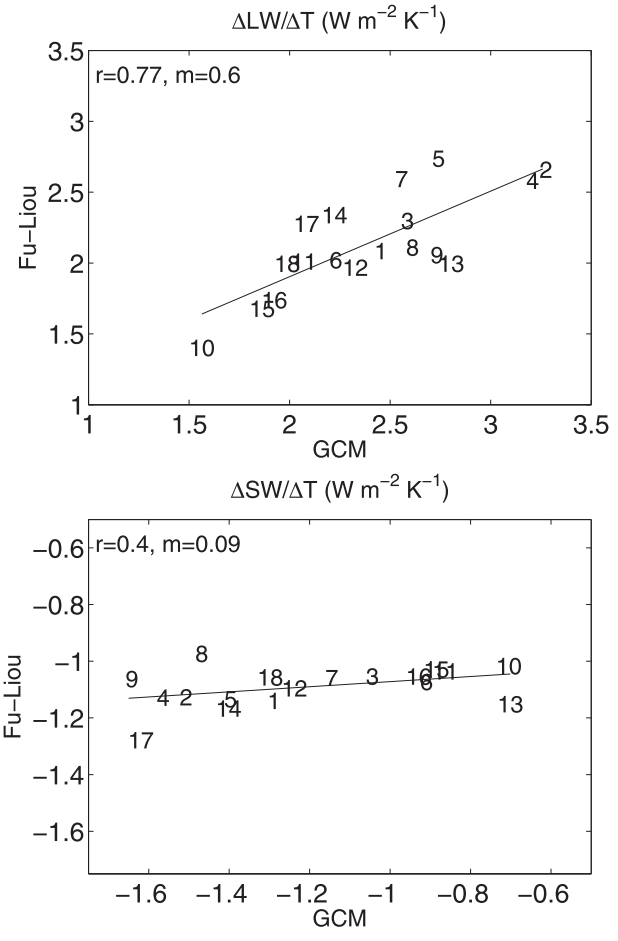

FIG. 7. Clear-sky atmospheric cooling change calculated from CMIP5 model output (GCM) and Fu and Liou (1992) column radiation code, using each model's change in temperature and moisture. Changes in (top) clear-sky LW cooling and (bottom) SW absorption normalized by global-mean surface temperature change.

$0.9\,\mathrm{W\,m^{-2}\,K^{-1}}$ in the GCM-calculated response. This suggests that much of the difference is due to different methods of computing SW heating in the CMIP5 models. Collins et al. (2006) compared GCM clear-sky radiative transfer calculations and found large differences in both SW and LW across models. Takahashi (2009a) also found differences in SW absorption between models in CMIP3. Their analysis suggested that the scatter in clear-sky SW absorption might be due to the spatial pattern of water vapor changes, but this is accounted for in our calculation and does not replicate the spread. For the remainder of this analysis we focus on the change in clear-sky LW atmospheric cooling.

It is well known that the lapse rate and water vapor feedbacks compensate each other at the TOA (e.g., Cess 1975; Zhang et al. 1994; Soden and Held 2006; Held and Shell 2012). Figure 8 shows our calculation of intermodel spread in the LW response to lapse rate and water vapor changes, and their sum, for each model, at the TOA and for the atmospheric column. At the TOA, the response to lapse rate and water vapor have similar spread but opposite sign. Their sum has a smaller spread than either individually. The total spread in TOA radiation is bigger than the sum of these two effects, indicating that other feedbacks also play an important role. Consistent with this compensation, the lapse rate and water vapor feedback are strongly anticorrelated ($r = -0.91$) with similar magnitudes of variation across models (slope $m = -0.76$, Fig. 9). If the responses scale across models as they do in the multimodel mean, then we can understand these responses from the calculations reported in on lines 8 and 9 (or 14 and 15), of Table 2. At the TOA, the response to changing lapse rate is comparable in magnitude and opposite in sign to the accompanying constant-RH moistening. There is also a contribution to the water vapor feedback from the moistening accompanying vertically uniform warming.

For the atmospheric cooling (Fig. 8), the story is different from the TOA. The atmospheric cooling responses to changes in lapse rate and water vapor have the same sign. The range of the sum of their responses has a magnitude similar to the response to lapse rate change alone. The range in the total clear-sky atmospheric radiative cooling is similar to the sum of these two effects, and to the change in precipitation. The relationship between the responses to moistening and changes in lapse rate has a weaker correlation ($r = -0.68$) and the

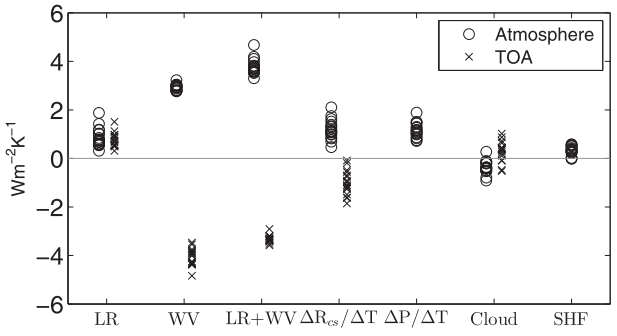

FIG. 8. Clear-sky radiative responses at the TOA (diagonal crosses) and for atmospheric cooling (circles) from different CMIP5 models. LW response to changes in lapse rate and water vapor are calculated with Fu and Liou (1992) radiative transfer code; ΔR_{cs}, cloud, sensible heat flux (SHF), and precipitation change are calculated directly from model output.

variation across models in the magnitude of the response to changing lapse rate is twice as large as water vapor (slope $m = -2.1$).

Why don't the responses to changing lapse rate and water vapor compensate for the atmospheric cooling? As for the TOA response, we can understand this in light of the calculations documented in Table 2. The response of atmospheric cooling to changes in lapse rate and the accompanying constant-RH moistening do compensate (Fig. 10); models with larger responses to changing lapse rate have smaller responses to changes in associated constant-RH moistening. However, the increased atmospheric cooling to the surface due to moistening that accompanies vertically uniform warming is twice as large as and of a different sign than that for the TOA response in the multimodel mean (Table 2), and is unrelated to the response to changes in lapse rate (Fig. 10). This increase in emission to the surface due to moistening is the largest component of the atmospheric cooling response to moistening. So the part of the response to moistening that compensates for changes in lapse rate is smaller than it is for the TOA response, and the sum of the two still has a substantial range.

It should be noted that these findings are different from those of O'Gorman et al. (2012), who find that the compensation between the response to water vapor and lapse rate changes does extend to the atmospheric cooling. Their response to lapse rate is comparable to ours, but their response to water vapor has the opposite sign. One important difference between the analyses is that they examine models forced by changes in aerosol forcing as well as greenhouse gases. Additional calculations with the same clear-sky radiative kernels (from Previdi 2010) indicate that our calculations have a larger increase in emission to the surface due to moistening than theirs. Their clear-sky response to multimodel

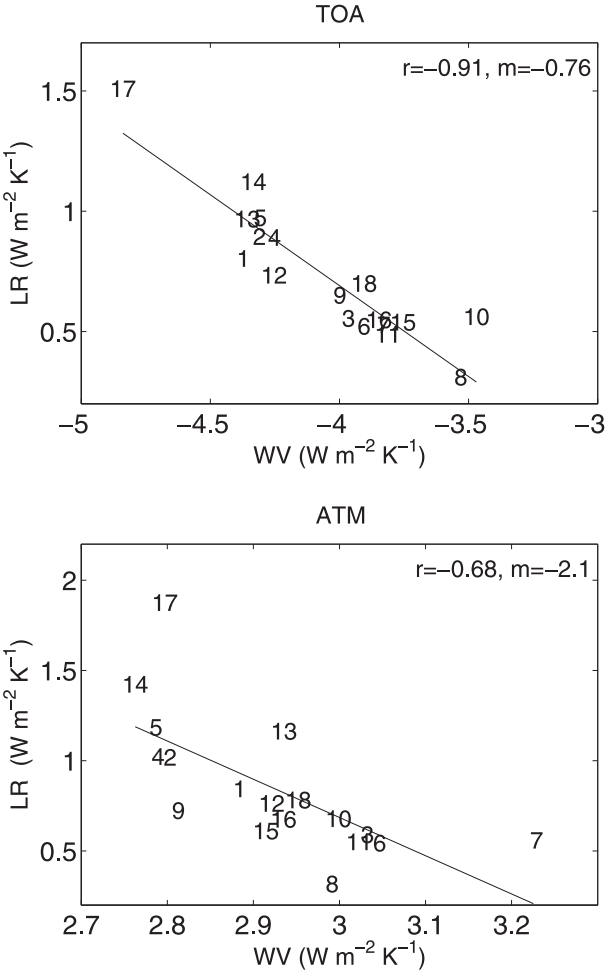

FIG. 9. The relationship between the LW response to changing lapse rate and water vapor in CMIP5 simulations from different models according to calculations with Fu and Liou (1992) column radiation model for the (top) TOA and (bottom) atmospheric column.

mean warming and moistening is 1.5 W m^{-2} K^{-1} smaller than ours.

The LW response to changes in lapse rate and moistening at constant RH, and the difference in SW absorption change across models each contribute to the intermodel spread in clear-sky atmospheric radiative cooling, and thus the rate of precipitation change. Changes in the cloud radiative effect are also a source of total-sky atmospheric cooling spread.

5. Discussion

a. Role of clouds and sensible heat flux

How do clouds play a role in precipitation change? Zelinka and Hartmann (2010) studied the LW cloud feedback (at the TOA) and showed that it is dominated by high clouds maintaining a constant cloud-top

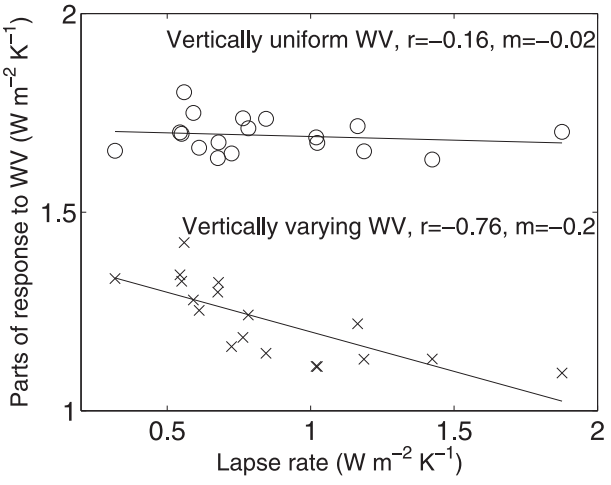

FIG. 10. The relationship between the LW atmospheric cooling response to changing lapse rate (LR) and vertically uniform (circles) and vertically varying (diagonal crosses) components of fixed-RH water vapor (WV) change in CMIP5 simulations from different models according to calculations with Fu and Liou (1992) radiative transfer code.

temperature as the climate warms. This maintains nearly constant LW emission to space from these clouds. In the case of atmospheric cooling, high clouds will not contribute to changing emission to space unless cloud fraction changes, and they will shield some of the changes in clear-sky LW emission to space, as we saw in section 3c. If high clouds decrease in area or get warmer, precipitation will increase more with warming than otherwise. The presence of high cloud will mitigate some of the increase in radiative cooling calculated in our idealized setting.

Low clouds, on the other hand, increase precipitation. If low cloud were to decrease with global warming, this simple calculation implies that this would result in decreased precipitation.

We can calculate the CMIP5 multimodel mean changes including clouds from total-sky TOA and surface radiative fluxes (rather than clear-sky values, as in the rest of this study). The change in total atmospheric radiative cooling is $0.8\,\mathrm{W\,m^{-2}\,K^{-1}}$. Subtracting the change in clear-sky radiative cooling from the total radiative cooling provides the change in atmospheric cloud radiative forcing, $-0.4\,\mathrm{W\,m^{-2}\,K^{-1}}$. This would reduce the precipitation increase compared to the clear-sky radiative response. The cloud radiative forcing change is driven by a change in LW cooling to the surface of $-0.9\,\mathrm{W\,m^{-2}\,K^{-1}}$, and is opposed by a change in LW cooling at the TOA of $0.4\,\mathrm{W\,m^{-2}\,K^{-1}}$and a change in SW cloud radiative forcing of $0.1\,\mathrm{W\,m^{-2}\,K^{-1}}$. Simple calculations presented in section 3c indicate that these are all consistent with a reduction in cloud fraction of both low and high clouds (Zelinka et al. 2012). Both changes in masking of clear-sky radiative cooling response and changes in the clouds themselves compose the cloud radiative forcing change.

In the multimodel mean of the transient CO_2 increase experiments (Table 1), sensible heat flux (from the surface to the atmosphere) decreases by $0.3\,\mathrm{W\,m^{-2}\,K^{-1}}$, or 30% of the precipitation increase. A reduction of sensible heat flux would support increased precipitation. This is a substantial but not dominant factor contributing to precipitation change. Coincidentally, perhaps, the changes in sensible heat flux and cloud radiative forcing nearly offset each other in this transient CO_2 increase experiment. Sensible heat flux plays a role in balancing global-mean precipitation change when changes in the climate state are very large (O'Gorman and Schneider 2008).

b. Role of aerosol forcing

The atmospheric energy budget perspective on precipitation change is useful for climate forcing agents other than CO_2. Black carbon is noteworthy because its TOA radiative forcing is small compared to its impact on precipitation change. Its main effect is to absorb SW in the atmosphere that otherwise would have been absorbed at the surface. While it causes warming as expected from its TOA radiative forcing, black carbon can dramatically reduce precipitation in ways that are not predictable from its TOA radiative forcing (Ming et al. 2010). Pendergrass and Hartmann (2012) showed that variation in black carbon forcing explains half of the variance across models in precipitation change in the A1b scenario of AR4. For black carbon, the atmospheric energy balance is a more reliable guide than the TOA perspective.

Another interesting situation in which the atmospheric energy perspective can guide us is stratospheric sulfate aerosol geoengineering. McCusker et al. (2012) performed an experiment in which global-mean surface temperature was held constant by increasing CO_2 while simultaneously increasing sulfate aerosol in the stratosphere just enough to compensate. In this experiment, precipitation decreased steadily as CO_2 and stratospheric sulfate aerosol increased. We need only one of the calculations from our framework, the CO_2 forcing, to explain this experimental result. The CO_2 forcing caused the atmospheric cooling rate to decrease. The temperature did not change, so the surface temperature-dependent responses of atmospheric radiative cooling also did not change. The sulfate aerosol acts by reflecting SW to space that would usually be absorbed at the surface, but this has little effect on the atmospheric energy budget and precipitation. The CO_2 forcing can be

viewed as directly suppressing the precipitation in this experiment, causing precipitation to decrease even without surface temperature change.

c. The surface energy perspective

In addition to the atmospheric radiative approach taken here, there are at least two other approaches to diagnosing the global-mean sensitivity of precipitation or evaporation to climate change: the surface radiation and the bulk flux perspectives. The bulk flux perspective is taken by Lorenz et al. (2010) and Richter and Xie (2008). Lorenz et al. (2010) differentiate the formula for bulk evaporative moisture flux from the ocean into terms depending on near-surface RH change, air–sea temperature difference change, and drag coefficient change (which includes changes due to near-surface wind speed). This approach paints a qualitatively different picture of surface turbulent moisture flux from the ocean, rather than radiative flux change globally (over land as well as ocean), but both diagnostic approaches must be physically consistent; moisture and energy fluxes must balance.

As for the surface and atmospheric radiative constraints, there are reasons to choose the atmospheric energy constraint on precipitation over the surface energy constraint on evaporation. First, clouds have a strong effect on SW radiation at the surface, whereas they only weakly affect the atmospheric SW balance. SW reflected by clouds can have an effect on precipitation primarily by cooling the planet. Lambert and Webb (2008) pointed out that the shortwave cloud feedback does not enter the atmospheric radiation budget as it does the TOA radiation budget, which is fortuitous since the SW cloud feedback is the most uncertain component of the TOA radiation budget. However, SW cloud feedback is very important for the surface and planetary energy budgets.

The changes in SW cloud forcing for the atmosphere and surface in the CMIP5 multimodel mean are comparable in magnitude: $0.1\,\mathrm{W\,m^{-2}\,K^{-1}}$ in the atmosphere and $0.2\,\mathrm{W\,m^{-2}\,K^{-1}}$ at the surface. But the range of these values across the models is telling. For the atmosphere, the range is $0.2\,\mathrm{W\,m^{-2}\,K^{-1}}$, while at the surface it is $2.0\,\mathrm{W\,m^{-2}\,K^{-1}}$, 10 times bigger.

Second, the surface heat capacity is bigger than the atmosphere's heat capacity, so the time scale for the surface to achieve balance is longer than the time scale for the atmosphere. For the surface to be in balance, we need to consider the ocean mixed layer, as well as deep circulation. The rate of change of storage in the ocean is estimated to be about $0.5\,\mathrm{W\,m^{-2}}$ at the present time (Loeb et al. 2012). The atmosphere equilibrates more quickly, so precipitation is more immediately constrained by the atmospheric budget.

6. Conclusions

Calculations with a column radiative transfer model and profiles of temperature and relative humidity quantify the sensitivity of the atmospheric cooling rate to uniform warming, upper tropospheric amplification of warming, constant relative humidity moistening, and CO_2 forcing. These calculations are used to understand the changes driving atmospheric cooling, which is the thermodynamic constraint on global-mean precipitation response to CO_2 forcing. The change in atmospheric cooling accounted for here is $1.2\,\mathrm{W\,m^{-2}\,K^{-1}}$ and includes the response to changing temperature, constant relative humidity moistening, and CO_2 increase. In CMIP5 transient CO_2 increase experiments, clear-sky atmospheric cooling increases by $1.2\,\mathrm{W\,m^{-2}\,K^{-1}}$, while precipitation increases by $1.1\,\mathrm{W\,m^{-2}\,K^{-1}}$.

In both idealized calculations and in global warming simulations with GCMs, the atmospheric cooling rate response is dominated by surface, rather than top-of-atmosphere, flux change. The dominant response at the surface is increased downward emission from the atmosphere, to which increases in water vapor in the lower troposphere make the dominant contribution. We expect that the underlying principles of this framework should extend to other forcings including aerosols and non-CO_2 greenhouse gases as well [as in Kvalevåg et al. (2013)].

Radiative responses to the presence of idealized clouds are calculated. High clouds suppress precipitation while low clouds enhance it. The change in GCM atmospheric column cloud radiative forcing (including both cloud feedback and change in cloud masking) due to CO_2 increase is $-0.4\,\mathrm{W\,m^{-2}\,K^{-1}}$, bringing the total atmospheric column radiative cooling increase to $0.8\,\mathrm{W\,m^{-2}\,K^{-1}}$.

We show that the intermodel spread in the rate of precipitation increase across the CMIP5 simulations can be attributed to differences in the atmospheric cooling. Clear-sky atmospheric shortwave absorption varies widely across models, due not to the spatial and temporal pattern of moistening, but more likely to differences in the formulation of shortwave absorption. The clear-sky atmospheric longwave cooling response to the changing lapse rate and water vapor contribute substantially to the intermodel spread in atmospheric cooling rate, in contrast to the top of the atmosphere. Cloud radiative forcing change has the same range of intermodel spread as each of the aforementioned components, but it is not significantly correlated with precipitation change. Changes in relative humidity are not an important contributor to intermodel spread.

This study demonstrates that a nearly sufficient framework to understand the atmospheric energy constraint on global-mean precipitation is the clear-sky response of the atmospheric radiation to changes in profiles of temperature and moisture and to CO_2 forcing. This framework connects precipitation changes to temperature and moisture changes through their role in the atmospheric energy budget. These connections provide a straightforward physical understanding of how and why global-mean precipitation increases with global warming at a rate much less than the increases in water vapor.

Acknowledgments. CMIP5 modeling groups provided simulations, and the resulting data were obtained from PCMDI. Bryce Harrop provided code for the insolation-weighted solar zenith angle calculation. Michael Previdi provided radiative feedback kernels for the atmospheric column. Three anonymous reviewers provided helpful feedback. This work was funded by NSF under Grant AGS-0960497.

REFERENCES

Allan, R. P., 2006: Variability in clear-sky longwave radiative cooling of the atmosphere. *J. Geophys. Res.,* **111,** D22105, doi:10.1029/2006JD007304.

Allen, M. R., and W. J. Ingram, 2002: Constraints on future changes in climate and the hydrologic cycle. *Nature,* **419,** 224–232, doi:10.1038/nature01092.

Cess, R. D., 1975: Global climate change: An investigation of atmospheric feedback mechanisms. *Tellus,* **27,** 193–198, doi:10.1111/j.2153-3490.1975.tb01672.x.

Collins, W., and Coauthors, 2006: Radiative forcing by well-mixed greenhouse gases: Estimates from climate models in the Intergovernmental Panel on Climate Change (IPCC) Fourth Assessment Report (AR4). *J. Geophys. Res.,* **111,** D14317, doi:10.1029/2005JD006713.

Costa, S. M. S., and K. P. Shine, 2012: Outgoing longwave radiation due to directly transmitted surface emission. *J. Atmos. Sci.,* **69,** 1865–1870.

Fu, Q., and K. N. Liou, 1992: On the correlated *k*-distribution method for radiative transfer in nonhomogeneous atmospheres. *J. Atmos. Sci.,* **49,** 2139–2156.

Held, I. M., and B. J. Soden, 2006: Robust responses of the hydrological cycle to global warming. *J. Climate,* **19,** 5686–5699.

——, and K. Shell, 2012: Using relative humidity as a state variable in climate feedback analysis. *J. Climate,* **25,** 2578–2582.

Inamdar, A., V. Ramanathan, and N. Loeb, 2004: Satellite observations of the water vapor greenhouse effect and column longwave cooling rates: Relative roles of the continuum and vibration-rotation to pure rotation bands. *J. Geophys. Res.,* **109,** D06104, doi:10.1029/2003JD003980.

Kvalevåg, M. M., B. H. Samset, and G. Myhre, 2013: Hydrological sensitivity to greenhouse gases and aerosols in a global climate model. *Geophys. Res. Lett.,* **40,** 1432–1438, doi:10.1002/grl.50318.

Lambert, F. H., and M. J. Webb, 2008: Dependency of global mean precipitation on surface temperature. *Geophys. Res. Lett.,* **35,** L16706, doi:10.1029/2008GL034838.

Loeb, N. G., J. M. Lyman, G. C. Johnson, R. P. Allan, D. R. Doelling, T. Wong, B. J. Soden, and G. L. Stephens, 2012: Observed changes in top-of-the-atmosphere radiation and upper-ocean heating consistent within uncertainty. *Nat. Geosci.,* **5,** 110–113, doi:10.1038/ngeo1375.

Lorenz, D. J., E. T. DeWeaver, and D. J. Vimont, 2010: Evaporation change and global warming: The role of net radiation and relative humidity. *J. Geophys. Res.,* **115,** D20118, doi:10.1029/2010JD013949.

McCusker, K. E., D. S. Battisti, and C. M. Bitz, 2012: The climate response to stratospheric sulfate injections and implications for addressing climate emergencies. *J. Climate,* **25,** 3096–3116.

Ming, Y., V. Ramaswamy, and G. Persad, 2010: Two opposing effects of absorbing aerosols on global-mean precipitation. *Geophys. Res. Lett.,* **37,** L13701, doi:10.1029/2010GL042895.

Mitchell, J. F. B., C. A. Wilson, and W. M. Cunnington, 1987: On CO_2 climate sensitivity and model dependence of results. *Quart. J. Roy. Meteor. Soc.,* **113,** 293–322, doi:10.1002/qj.49711347517.

O'Gorman, P. A., and T. Schneider, 2008: The hydrological cycle over a wide range of climates simulated with an idealized GCM. *J. Climate,* **21,** 3815–3832.

——, R. P. Allan, M. P. Byrne, and M. Previdi, 2012: Energetic constraints on precipitation under climate change. *Surv. Geophys.,* **33,** 585–608, doi:10.1007/s10712-011-9159-6.

Pendergrass, A. G., and D. L. Hartmann, 2012: Global-mean precipitation and black carbon in AR4 simulations. *Geophys. Res. Lett.,* **39,** L01703, doi:10.1029/2011GL050067.

Previdi, M., 2010: Radiative feedbacks on global precipitation. *Environ. Res. Lett.,* **5,** 025211, doi:10.1088/1748-9326/5/2/025211.

Richter, I., and S.-P. Xie, 2008: Muted precipitation increase in global warming simulations: A surface evaporation perspective. *J. Geophys. Res.,* **113,** D24118, doi:10.1029/2008JD010561.

Soden, B. J., and I. M. Held, 2006: An assessment of climate feedbacks in coupled ocean–atmosphere models. *J. Climate,* **19,** 3354–3360.

Stephens, G. L., and T. D. Ellis, 2008: Controls of global-mean precipitation increases in global warming GCM experiments. *J. Climate,* **21,** 6141–6155.

Takahashi, K., 2009a: The global hydrological cycle and atmospheric shortwave absorption in climate models under CO_2 forcing. *J. Climate,* **22,** 5667–5675.

——, 2009b: Radiative constraints on the hydrological cycle in an idealized radiative–convective equilibrium model. *J. Atmos. Sci.,* **66,** 77–91.

Taylor, K. E., R. J. Stouffer, and G. A. Meehl, 2012: An overview of CMIP5 and the experiment design. *Bull. Amer. Meteor. Soc.,* **93,** 485–498.

Zelinka, M. D., and D. L. Hartmann, 2010: Why is longwave cloud feedback positive? *J. Geophys. Res.,* **115,** D16117, doi:10.1029/2010JD013817.

——, S. A. Klein, and D. L. Hartmann, 2012: Computing and partitioning cloud feedbacks using cloud property histograms. Part II: Attribution to changes in cloud amount, altitude, and optical depth. *J. Climate,* **25,** 3736–3754.

Zhang, M., J. Hack, J. Kiehl, and R. Cess, 1994: Diagnostic study of climate feedback processes in atmospheric general circulation models. *J. Geophys. Res.,* **99** (D3), 5525–5537.